New Materials, Compounds and Applications
Vol.8, No.2, 2024, pp.199-222
https://doi.org/10.62476/nmca82199

SYNTHESIS AND CHARACTERIZATION OF LASER-ABLATED SILVER AND TITANIUM OXIDE NANOPARTICLES: IMPLICATIONS FOR DRUG DELIVERY

Walaa A. Salih*, Alaa Al-Taie

Department of Biomedical Engineering, College of Engineering, Al-Nahrain University, Baghdad, Iraq

Abstract. Using the laser ablation method, the study explores the synthesis and characterisation of three nanocomposites: titanium dioxide (TiO_2)/polyethylene glycol (PEG), silver (Ag)/titanium dioxide (TiO_2)/polyethylene glycol (PEG) and silver (Ag)/titanium dioxide (TiO_2)/chitosan (Ct's). These composites act as delivery systems for 5-Fluorouracil (5Fu), an anticancer medication. Various characterization techniques were utilised, such as Fourier transform infrared spectroscopy, UV-visible, X-ray diffraction analysis and transmission electron microscopy. The results show that the freshly produced composites have chemical interactions; the Ag-TiO2-PEG-5Fu composite has the highest crystallinity. Particle size distribution has an average size of 45 nm and a range of 10 to 100 nm. The UV-visible absorption spectrum shows a clear blue shift, which improves the possibility for medication delivery.

Through cytotoxicity tests on the AMN3 cell line, the study illustrates the promise of nanocomposites in pharmaceutical applications, particularly in boosting the efficacy of cancer therapy. The co-administration of polymers with 5-FU augments their cytotoxic effect, indicating viable substitutes for the treatment of cancer. The $AgTiO_2$ PEG 5-Fu composite, in particular, has the strongest cytotoxic effects, suggesting that it is a viable therapy option for cancer. PEGylation improves medication dispersion, which raises cytotoxicity slightly. Chitosan demonstrates inherent anti-tumorogenic properties at particular dosage ranges. Furthermore, decreasing cytotoxicity by doubling the content of silver (Ag) in the $AgTiO_2$ PEG 5-FU composite may be attributed to Ag particle agglomeration. It's interesting to note that when compared to the $AgTiO_2$ composite, the TiO_2 composite shows noticeably more cytotoxicity. All things considered, the study highlights the potential of nanocomposites in drug delivery applications, especially when it comes to improving the administration of anticancer drugs. The combination of polymers, nanometallic materials and 5-FU offers bright futures for cancer treatment; positive results have been seen even in created composites that do not include 5-FU.

Keywords: *Silver nanoparticles, titanium dioxide nanoparticles, polyethylene glycol, chitosan, polyethylene Glycol, 5Fu, nanomaterial characterizations.*

Corresponding Author: *Walaa A. Salih, Department of Biomedical Engineering, College of Engineering, Al-Nahrain University, Baghdad, Iraq, e-mail: st.walaa.a.salih@ced.nahrainuniv.edu.iq, walaa.a1812@gmail.com*

Received: *23 October 2024;* ***Accepted:*** *22 April 2024;* ***Published:*** *2 August 2024.*

1. Introduction

Nanotechnology is a new topic among the scientific community, however, the term itself is not new. It is based on the study of molecules, structures and substances with

How to cite (APA):
Salih, W.A., Al-Taie, A. (2024). Synthesis and characterization of laser-ablated silver and titanium oxide nanoparticles: Implications for drug delivery. *New Materials, Compounds and Applications, 8*(2), 199-122 https://doi.org/10.62476/nmca82199

nanoscale dimensions, known as nanoparticles (NPs). Due to their extraordinarily high surface-to-volume ratio, nanoparticles (NPs) feature a number of physicochemical traits that are not often found in their comparable bulk materials. The atom's number on the NPs surface raises the thermo-dynamic stability of the NPs. when the NPs are exposed to a temperature gradient, however, the presence of fewer atoms in the bulk material results in a less well-defined phase transition (Roduner, 2006). It has been discovered that as the ratio of the surface area to the volume of nanoparticles increases and as a result, the dominating attitude of the atoms on its surface likewise changes, which is a significant to consideration in the formation of their distinctive properties (Mathew *et al*., 2010). The greater ratio also confers remarkable catalytic reactivity because it supplies adequate binding sites for substrates during chemical reactions (Cuenya, 2010). The technique of eliminating fabric from a surface by means of the application of strong laser irradiation is referred to as laser ablation. The term "laser ablation" was derived from the Latin word "ablation", which means removal. PLAL (Pulse laser ablation in liquid) media may be a promising method to prepare nanomaterials by ablated species reacting at the plasma-liquid contact (Sasaki *et al*., 2006). According to PLAL, the laser-material interaction mechanism employing various liquid media has numerous benefits. First, the range of target materials and liquid environments allows for the production of a vast array of final products. Alterations in laser parameters or the type of liquid medium can alter the nanostructure's size and morphology (Messina, 2013; Škorc *et al*., 2010). Second, a simple procedure that produces topically applied products without additional purification. A type of experimental equipment is inexpensive and its parameters are simple to manipulate. The facility also provides favorable pressure and temperature conditions for metastable phases, the experiment serves to demonstrate the technique's capacity to produce nano-sized materials, which can not be manufactured using existing methods. Finally, colloidal nanoparticle suspensions were maintained in liquid media. Although liquid laser ablation has few practical limitations, it is still difficult to precisely control the size distribution of the generated nanoparticles (Kong *et al*., 2017; Maaspuro, 2021; Titov *et al*., 2012). Creating nanoparticles in the liquid environment by laser-ablation of a solid object is considered as a "green" a process for producing nanoparticles at a large-scale and with tailored features (Semaltianos *et al*., 2009). Several studies have elucidated the potential applications and benefits of laser ablation in nanoparticle synthesis. For instance, Khashan et al. (2021) prepared TiO_2 NP suspension in deionized water using laser ablation in liquid by a Q-switch Nd: YAG laser at various laser energies and ablation durations. UV-visible absorptions spectra were gained using a UV-Vis (UV-Visible spectrophotometer), FTIR (Fourier-transform infrared), XRD (X-ray diffraction) and TEM (transmission electron microscopy) were used to characterize the samples. UV-V is spectra revealed TiO_2 NPs' distinctive in UV range from band to band of peak absorption. The presence of an O-Ti-O bond was shown by FTIR research. XRD patterns revealed the existence of TiO_2 (101) and (112) crystalline phase. According to TEM images, TiO_2 NPs relying on the ablation duration, have a spherical-like form with various size patterns. Additionally, it was shown that there was a relationship between the laser ablation duration and the size distribution of TiO2 NP, with longer ablation durations leading to a lower size dispersion (Khashan *et al*., 2021). Tsuji et al. (2002) silver nanoparticles have been produced in water by laser ablation employing wavelengths of (355, 532 and 1064) nm with a reasonably high fluence at 36 J/cm^2. The spherical form of these nanoparticles does not change (independent of the ablation light wavelength), as observed in TEM and absorption spectra acquired with a spectrometer

(Tsuji *et al*., 2002). Boutinguiza et al. (2015) improved manufacturing yield through open-air laser ablation of silver-plates with a nanosecond laser. The outcomes showed that nanoparticles of crystalline-silver rounded forms and restricted size distributions ranged from a few to (50) nm could be produced. The acquired nanoparticles formed in an explosive phase as their primary process, which encouraged the creation of assemblies with chain-like particles and continuous crystalline interfaces between particles. (Boutinguiza *et al*., 2015). Barreca et al. (2010) used laser ablation method to create titanium dioxide nanoparticles in purified H_2O solution. The tests were carried out by irradiating a Ti target with a 532 nm of an Nd-YAG laser output while changing the operative fluence between (1 to 10) J cm^2 and the ablation duration between (10 and 30) minutes. Agglomerations of (100 to 200) nm, the content of which increases with laser fluence and nanoparticles with diameters less than 10 nm were both seen using an electron microscope. UV-vis absorbance observations show that the optical bandgap values are compatible with the anatase phase (Barreca *et al*., 2010). Fernández-Arias et al. (2019) used PLAL (Pulsed laser ablation in liquid) to create silver nanostructured. The topography, composition, structure of crystals, topography of the surface and optical characteristics of the generated films were investigated using EDS (energy dispersive X-ray spectroscopy), HRTEM (high resolution transmission electron microscopy), Ultraviolet–visible spectrophotometry, and XRD (X-ray diffraction). Ag nanoparticles with sizes between a few and several hundred nanometers made up the coatings. At (400) nm, the films showed exhibited a distinct localized surface plasmon resonance (LSPR) and a homogeneous shape and appearance (Fernández-Arias *et al*., 2019). Tajdidzadeh et al. (2014) also examined Ag-NPs' particle size, shape, and stability. Using an Nd-YAG pulsing laser with (532) nm wavelength and (360) mJ/pulse of energy, pure Ag plates were ablated to produce Ag-NPs in organic substances like EG (ethylene glycol) and biopolymers including chitosan. The mediums (EG, chitosan) allowed for the creation of NPs that were evenly disseminated, with an average size of around (10) nm for chitosan and (22) nm for EG. The stability, shape and particle size of NPs were evaluated in comparison to pure water. By evaluating the samples' UV-visible absorption spectra, the stability of the samples was investigated. The findings showed that chitosan had a greater rate of NP production than other mediums (Tajdidzadeh *et al*., 2014). Pulse laser ablation of submerged Au, Ag, and Cu metal objects, were used by Herbani et al. (2018) metal and oxide nanoparticles were manufactured. Due to the fast oxidation of Cu in water, which led to its poor durability, they discovered CuO nanoparticles for the Cu target. Due to their unique colors—red, yellow, and dark green colloidal suspensions, respectively — the creation of Au, Ag and CuO nanoparticles could hardly be distinguished by the unaided eye. Additionally, the UV-Vis spectrophotometer was used to confirm that the surface plasmon frequency of Au, Ag and CuO colloidal nanoparticles is at 520, 400 and 620 nm, respectively. All of the manufactured nanoparticles had crystalline shapes and particle diameters between 20 and 40 nm, according to TEM analysis (Herbani *et al*., 2018). These studies underscore the diverse applications and potential of laser ablation in nanoparticle synthesis for various fields, including biomedicine and materials science. Furthermore, recent research has focused on incorporating nanoparticles into drug delivery systems for enhanced therapeutic efficacy, Narmani et al. (2020) by using PEG-PAMMA G_4-FA-5-FU -^{99m}Tc In-vivo studies on female mice. The mice were monitored daily for tumor onset and tumor inhibition studies were performed when tumor volume reached 619.2 ± 98.5 mm^3, the study evaluated drug release behavior, stability, cancer cell inhibition ability and tumor inhibition potency of FA-targeted nanoparticles in breast

cancer cells, revealing their actual efficiency (Narmani *et al*., 2020). Sağir et al. (2016) successfully loaded 5-Fluorouracil into a magnetic zeolite-magnetite nanocomposite (MZNC) to create a fluorescent hybrid nanoparticle with near-infrared optical properties they found that MZNC could be an effective carrier for 5-FU and also targeted to tumor sites (Sağir *et al*., 2016), Safwat et al. (2018) studied incorporated 5-FU/CTAB-GNPs into Pluronic F127 gel to enhance skin application. The gel was prepared using a cold method and In vivo testing demonstrated the cream preparation's significant anti-skin cancer impact, demonstrating its potential for topical delivery with reduced side effects, improved therapeutic efficacy, and improved patient compliance (Safwat *et al*., 2018). Nazir et al. (2021) described the manufacture of a nanodrug as well as its inclusion into a polymeric matrix of Functionalized arabinoxylan (CMARX), which was synthesized from Plantago Ovata in a variety of forms. In order to investigate a wide range of physicochemical properties and in-vitro activities, the nanodrug (5-Fu) is first loaded into CMARX and then it is subjected to crosslinking with varied concentrations of the crosslinker tetraethoxysilane (TEOS). There has been a wide range of wetting reactions seen in nanocomposite hydrogels. This results in distinct swelling and biodegradation behavior, which is critical for the continuous release of 5-Fu (Nazir *et al*., 2021). The findings from these studies suggest that there is merit in investigating the properties of polymer-nanometallic materials created through laser ablation of a new developed 5-Fu loaded nanocomposites for cancer treatment purposes. This study explores the use of pulse laser ablation in liquid (PLAL) alongside polymers and drugs, presenting an opportunity to examine the potential of nanocomposites for targeted drug delivery systems. Such systems could be evaluated for their capability to deliver therapeutic substances directly to cancer cells, offering promising prospects for improving cancer treatment.

2. Materials and Methods

2.1. Materials

Poly ethylene glycols PEG 6000 g/m from (Hebei Iversion Biotechnology Co. Ltd, China), of chitosan with a purity of 95.7% from (Hongwu International group, China), Average particle size (APS) : ≤ 80 nm with spherical shape, (1×1) cm^2 silver plate (purity 99.99%) and titanium sheet (1×1) cm^2 and distilled water were purchased from the local market in Baghdad, Iraq.

2.1. Methods

The creation and manipulation of nanomaterials in liquid using laser irradiation is a rapidly expanding field. The synthesis of the developed composites are as follows:

2.1.1. Synthesis of nanoparticles

(1×1) cm^2 of silver plate was firstly washed with acetone in ultrasonic water bath to remove any pollutants and to activate the surface before the laser ablation process. The silver alloy was then immersed in 100 ml of deionized water and the laser beam (Nd-YaG) was adopted with 200 pulses of 600 mJ and 10 Hz. The color of the solution was immediately changed to yellow which confirms the formation of silver nanoparticles. The silver nanoparticles were collected by centrifuging the mixture at 13000 rpm at 7^oC

(Zeng *et al*., 2012). The same procedure was used to synthesize TiO_2 nanoparticles, but the laser beam parameters were 100 pulses of 4 mJ and 15 Hz (Shukri *et al*., 2018).

2.2.2. Synthesis of (Ag(X)TiO$_2$(X) -PEG, Ag(2X) TiO$_2$(X) -PEG and TiO$_2$-PEG) nanocomposites

These composites were synthesized by green sonochemistry. 100 mM of Ag nanoparticles in 2 ml of PEG was mixed with 50 mM or 100 mM of TiO_2 nanoparticles in 2 ml of PEG under vigorous stirring to form yellowish-white mixture. For one hour, the mixture was stirred at room temperature at a speed of 700 rpm, followed by sonication using the ultrasonic probe (probe 6, 150 W) for 10 minutes at 25-35^o C. The same procedure was used to synthesize TiO_2-PEG without using Ag.

2.2.3. Synthesis of (Ag(X)TiO$_2$(X) -Chitosan) nanocomposites

This composite was also synthesized by green sonochemistry. 100 mM of Ag nanoparticles in 2 ml of chitosan (1 g of chitosan in 50 ml of 0.5% acetic acid) was mixed with 100 mM of TiO_2 nanoparticles in 2 ml of chitosan under vigorous stirring to form deep yellow mixture. For one hour, the mixture was stirred at the temperature of the room at a speed of 700 rpm. The mixture was sonicated in ultrasonic probe (probe 6, 150 W) for 10 minutes at 25-35 ^{o}C. All mixtures in (2.1, 2.2 and 2.3) were then filtered using 220 nm filter Millipore. The overall procedure shown in Figure 1.

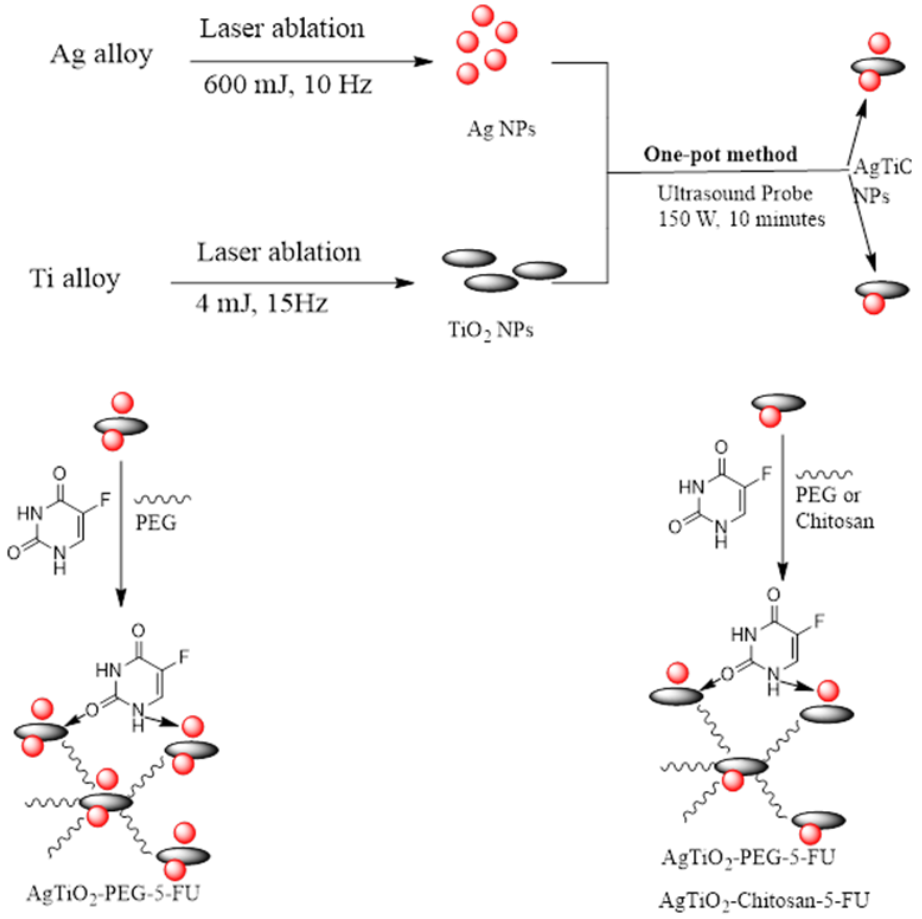

Figure 1. The overall process of the synthesis of nanocomposite

3. Cell Line Preparation

AMN3 cells lines were supplied from the Iraqi Canter for Cancer and Medical Genetic Research (ICCMGR), experimental therapy department, cell bank unit, Al-Mustansiriyah University. The following steps illustrate the cell line preparation method.

3.1. Maintenance and subculture of cells

The RPMI-1640 medium was purchased from US Biological and used to cultivate the (AMN3) cell line. 10% fetal bovine serum (FBS), 100 units/mL of penicillin and 100 g/mL of streptomycin were added to the medium as supplements. These supplements offer vital nutrients and foster a favourable environment for cell development. The cells were grown in adherent confluent monolayers, which means they were affixed to the surface of the culture vessel in a single layer. Cell growth and nutrient absorption are made possible as a result. The cells were kept at a constant temperature of 37 °C in a humid environment that contained 5% CO_2. The circumstances for cell development and viability in this environment were ideal. The cells were harvested after a quick trypsinization process using trypsin-EDTA solution from Capricorn-Scientific, Germany. Trypsin is an enzyme that causes the cells' connecting proteins to disintegrate, enabling the cells to separate from the culture surface. To assist balance the activity of the trypsin solution and guard against cell harm, EDTA (ethylenediaminetetraacetic acid) was added. Easy and quick cell separation from the culture medium was made possible by this trypsin-EDTA treatment, allowing for later analysis or testing. In RPMI-1640 media supplemented with FBS, penicillin and streptomycin, the (AMN3) cell line was grown. At 37 °C, the cells were cultivated in adherent monolayers and a humidified 5% CO_2 environment. Cells were harvested by quickly treating with trypsin-EDTA to separate them from the culture surface (Al-Ziaydi *et al*., 2020; Al-Ziaydi *et al*., 2020)

3.2. Cytotoxicity assays

AMN3 cells were plated in 96-well plates at a density of 7000 cells/well to test the MTT assay's ability to detect the cell-killing effects of nanocomposites material. When a confluent monolayer had formed after 24 hours, the cells were exposed to nanocomposites material ($AgTiO_2$ PEG 5-FU, TiO_2 PEG 5-FU, $2AgTiO_2$ PEG 5-FU, $AgTiO_2$ Chitosan 5-FU, TiO_2 Chitosan 5-FU, $AgTiO_2$ PEG, TiO_2 PEG, $2AgTiO_2$ PEG and $AgTiO_2$ Chitosan), at doses of 100, 50, 25, 12.5, 6.25 and 3.125 g/mL. Following a treatment period of 72 hours, cell viability was evaluated. Following a treatment period of 72 hours, the media was subsequently extracted from every well of the cell growth plate. Following that, a volume of 28 µL of a 2 mg/mL solution of MTT (3-(4,5-dimethylthiazol-2-yl)-2,5-diphenyltetrazolium bromide) was introduced into every well. Subsequently, the cells were subjected to incubation at a temperature of 37 °C for a duration of 2.5 hours, therefore facilitating the generation of formazan crystals, which are indicative of the presence of live cells. After the incubation period, the MTT solution was meticulously extracted from the wells. Subsequently, a volume of 130 µL of Dimethyl Sulfoxide (DMSO) was introduced into each well in order to facilitate the dissolution of any remaining formazan crystals. In order to achieve complete solubilization, the plate was subjected to further incubation at a temperature of 37 °C for a duration of 15 minutes, with simultaneous agitation. The absorbance at 492 nm was

measured using a microplate reader to detect the cell viability and cytotoxic effects of the treatments.

To calculate the inhibition rate of cell growth (percentage of cytotoxicity), you can use the following equation:

$$Inhibition\ rate\ = A - B/A * 100 \quad (1)$$

where A is the optical density of control and B is the optical density of the samples. The percentage of cytotoxicity at each concentration of AMN3 material can be estimated by examining the absorbance values obtained from the MTT experiment (Al-Salman *et al*., 2020; Al-Shammari *et al*., 2020; Al-Ziaydi *et al*., 2020).

3.3. Statistical analysis:

GraphPad Prism 6 software was used to statistically analyse the acquired data using an Analysis of Variance (ANOVA). The Analysis of Variance (ANOVA) is a frequently employed statistical technique for examining variations between samples. To find out if there are significant differences between the means of three or more groups, an ANOVA is used. ANOVA determines if any observed differences are statistically significant by contrasting the variance within each group to the variation between the groups (Bahjat *et al*., 2021; Jabir *et al*., 2017). Following ANOVA, Tukey's multiple comparison test was chosen as a post-hoc analysis.

4. Characterization of Nanocomposite

The absorption spectrum of synthesized nanocomposites was obtained using SHIMADZU UV-VIS (1900i/ Japan) spectrophotometer which showed surface plasmon resonance (SPR) bands. Fourier transform infrared spectroscopy (FTIR) spectra was performed by SHIMADZU IR Affinity (-1 plus / Japan) spectrometer using potassium bromide pellets (400 – 4000) cm−1.TEM (Zeiss-EM10C-100 KV) was used for the morphological observation of composites. The analysis of the XRD was recorded using a wide-angle X-ray diffractometer (Panalytical X-Ray Diffractometer, model-X'pert Powder) utilizing the radiation of Cu Kα. The XRD was collected at room temperature.

5. Results and Discussion

5.1. UV-Visible spectral analysis

The shape, size, free electron density and interactions of NPs improve their spectrum plasmon surface resonance. This illustrates that the UV-spectroscope is a dependable tool for monitoring and detecting NP aggregation and electron injection (Kumar, 2013). The spectra show noticeable absorption peaks for silver nanoparticles' surface plasmon resonance (SPR) absorption at 420nm as shown in Figure (2a) which is agreed with previous studies (Kumar, 2013), while Figure (2b) shows the spectra of TiO_2, the studied spectra was between (190 and 1100) nm and it has shown a peak at 360nm wavelength , this agrees with Khashan et al. (2021) study that found the UV spectra of TiO_2 around 360 nm. Figure (2c) shows the band between (202- 266) nm which contains TiO_2, PEG and 5Fu, there is a clear blue shift which may be related to the reduction of the particle size due to the linking between metallic nanoparticles, PEG and

5Fu. According to the previous studies the UV–vis absorption spectrum of the 5Fu is at 266nm (Qin *et al*., 2012; Tomoiaga *et al*., 2013) while the TiO_2 at 350nm (Praveen *et al*., 2014). Figure (2d) shows that there is an overlapping between TiO_2 , PEG and 5Fu peaks, a shift of the reflectance spectrum of Ag-TiO_2-PEG-5Fu towards the lower wavelength region was observed which is matched with previous research (Praveen *et al*., 2014), where the absorption edge shifted to 204 and 266 nm. Evidently, there is a blue shift, this supports the Mie theory's prediction that NPs develop more effectively and their size is reduced (Tajdidzadeh *et al*., 2014). The UV–vis absorption spectrum for the Ag is at 446 nm while the TiO_2 at 290nm, there is an overlapping between TiO_2, PEG and 5Fu peaks at an observed band between (450-946) nm as shown in Figure (2e). The Ag absorption peak appears because its concentration has doubled. Figure (2f) shows the UV–Vis absorption spectra of Ag-TiO_2-chitosan-5Fu nanocomposite, where the observed peaks are at 204 nm and 266 nm. This can be attributed to the overlapping of absorption bands of TiO_2, chitosan and 5Fu. It is clear that there is a blue shift, which also demonstrates an improvement in the NPs' formation efficiency and implies a reduction in particle size in accordance with the Mie theory. This decrease in particle size is explained by the laser-induced coupling of PEG molecules and metallic nanoparticles. Here, Chitosan molecules engage with atoms of silver and titanium (Tajdidzadeh *et al*., 2014).

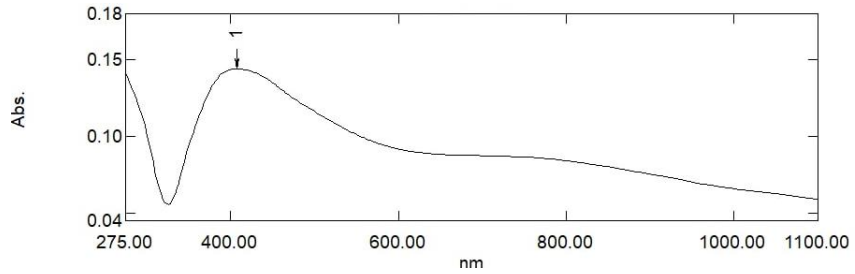

(a)

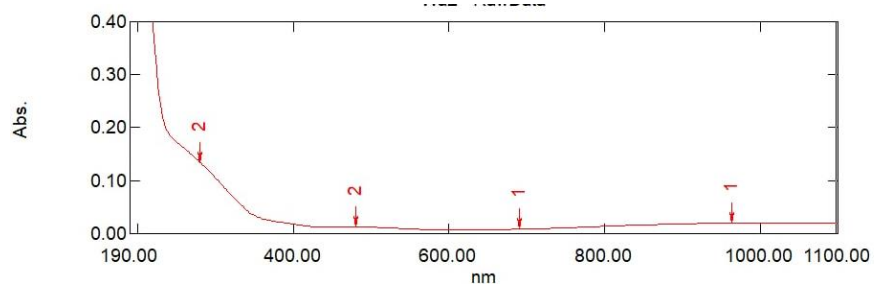

(b)

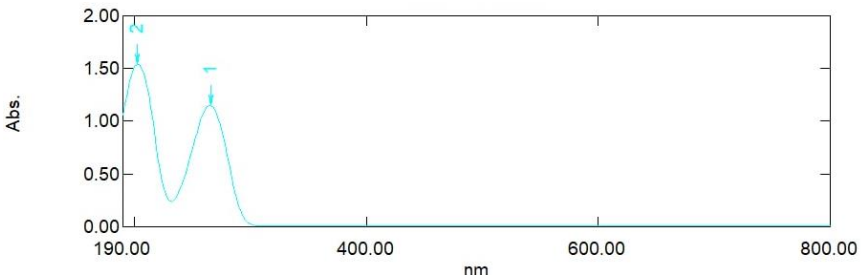

(c)

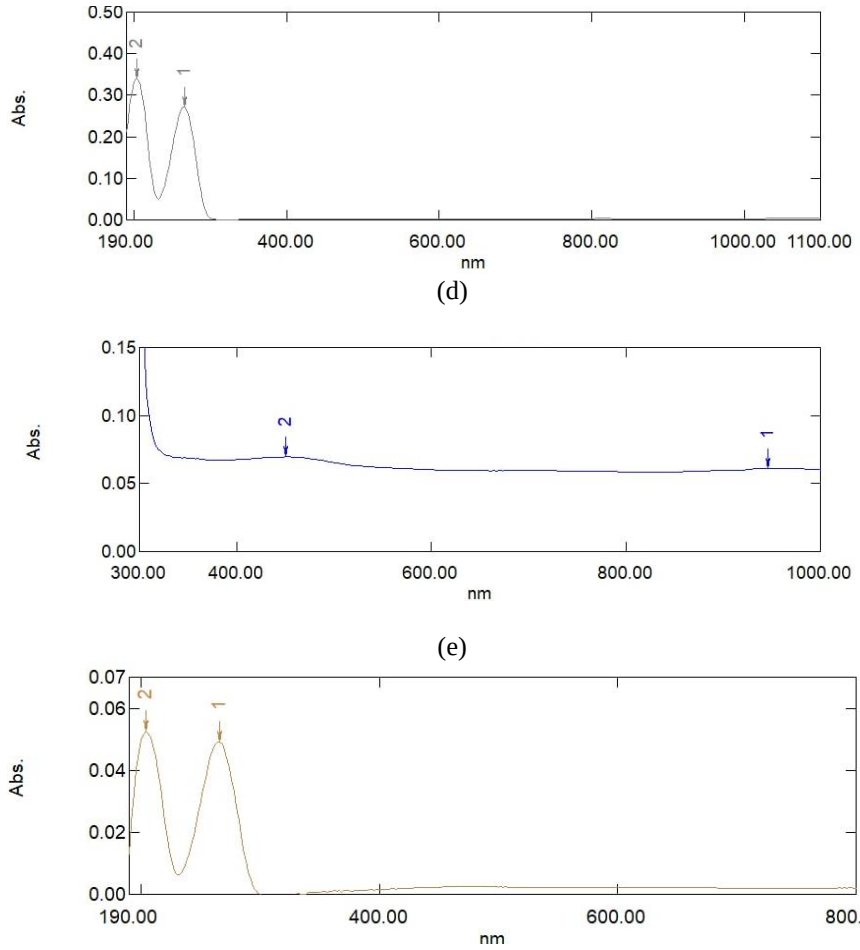

Figure 2. UV-absorption spectrum of aqueous (a) silver nanoparticles, (b) TiO_2 nanoparticles, (c)TiO_2-PEG-5Fu nanocomposite, (d) $AgTiO_2$ PEG 5Fu; (e) ($2AgTiO_2$) PEG 5Fu and (f) $AgTiO_2$ chitosan 5Fu synthesized by laser ablation method

5.2. Fourier transforms infrared spectroscopy (FTIR) analysis

Fourier transform infrared (FTIR) spectroscopy is a valuable instrument for determining chemical compounds in gases, liquids, powders and films based on their structural groups. Figure (3a) shows the Functional groups contained in the (Ag-TiO_2-PEG-5Fu) nanocomposite. A peak at (2831.50) cm^{-1} exhibits the stretching of C-H, while that at (2349) cm^{-1} shows O=C=O stretching in the bond, suggesting that there are carbon dioxide molecules. A powerFul peak at (1720.50) cm^{-1} is for stretching of C-H and considered a sign for carboxylic acid. The peak at (1986.68) cm^{-1} is referred to the C=C=C stretching of allene. The peak at (2596.18) cm^{-1} represents poor stretching of S-H of thiol, while that at (1720) cm^{-1} exhibits a potent stretching of C=O of vibration of conjugated anhydride. A weak stretching of C=C assignable to tertiary amide was clearly seen at the peak of (1662.62) cm^{-1}, while it indicates N-O stretching at (1500.62) cm^{-1} and the other at (1450.47) cm^{-1} exhibits the strong N-O bending representing nitro compounds. S=O strong stretching sulfonyl chloride is obvious at (1384.89) cm^{-1}. The peak at (1099.43) cm^{-1} demonstrates significant C-O stretching of primary-alcohol, whereas peaks at (991.41) cm^{-1} and (883.40) cm^{-1} exhibit C=C bending of strong alkene and 813.96 cm^{-1}

represents medium bending alkene the composite samples show a peak at (1654.92) cm^{-1}. The carbonyl-groups created by the interaction between the Ag ions and the C-O-H and the subsequent reduction in the ions of the metal to generate metal nanoparticles are represented by this band (Fahmy *et al*., 2015). PEG is clearly seen at the wavelengths of (2877.79), (1350.62) and (1099.43) cm^{-1}, which are corresponding to the stretching of the C-H, bending of C-H and the stretching vibrations of C-O. All of those bands have been moved from their initial places in PEG, indicating the nature of hydrogen bonds and verifying the interaction of PEG with the surface of TiO_2 NPs (Ramlli *et al*., 2017). Broad band between the (3066.82) and (3402.43) cm^{-1}, is attributed to—NH stretching vibrations in the spectrum of 5Fu (MERVE et al., 2012). Concerning Figure (3b), the vibratory stretching of the hydroxyl group within the TiO_2 nanoparticle causes the spectroscopic band that was seen at (3390.86) cm^{-1}. The bending modes of water absorbed and Ti-OH is shown by the peak values at (1654) cm^{-1} and (1716) cm^{-1}, respectively. The peak value at (466) cm^{-1} is corresponding to the Ti-O-Ti, while the peaks over (420–1246.02) cm^{-1} are referred as the characteristic of O-Ti-O modes. The intense peak at (640.37) cm^{-1} is assigned to the Ti-O stretching band which is the characteristic peak of TiO_2 (Al-Amin *et al*., 2016). The appearance of characteristic absorption peaks of PEG such as C-O-C (antisymmetric stretching) is at (1350.17) cm^{-1} and -CH (out-of-plane bending) is at (955.27) cm^{-1}. Peaks within the FTIR spectra of PEG as well as PEG-coated nanoparticles of TiO_2 (1099.43, 1229 and 2872) cm^{-1} peak indicated that PEG was grafted to the nanoparticles. The peak with (2877.79) cm^{-1} in the PEG spectra is associated with -CH2 stretching vibrations. It is moved at 2872) cm^{-1} in PEG-coated TiO_2 nanoparticles. This demonstrates the nature of hydrogen bonds. Within both PEG and PEG-coated Titanium dioxide nanoparticles, peaks at (1099.43) cm^{-1} corresponds to the stretching vibration of -C-O-C- (Venkatasubbu *et al*., 2013). Peaks within (1543.05 and 1720) cm^{-1} are due to polymer bleaching and C-O-C bonds. Additional findings indicated that the stretching vibrations of -OH groups and the stretching of C-H may be determined from the peaks at (3352.88, 2931.80 and 1091.71) cm^{-1}. Because of the existence of C-O -C, the C-F (fluoro-compound) exhibited a tiny peak within the anomeric region (945.12 - 752.24) cm^{-1}. Due to a beneficial interaction that exists between the medication and its nano-carrier, the stretching vibration of CO at (1670.35) cm^{-1} may be explained. Additionally, an overlap occurs between O-H & N-H (primary amine) bonds of 5Fu possibly demonstrated a band at about 2827.64–3552.88 cm^{-1}, this is agrees with another study (Anirudhan *et al*., 2015). By comparing Figure (3c) and Figure (3a), Figure (3c) represents 2Ag-TiO_2-PEG-5Fu which is the same nanocomposite shown in Figure (3a) but with double concentration of Ag. It was noticed that the most peaks and bands stay the same with a very small shift. As indicated in Figure (3d), As a result of the stretching group of [-NH2] & [-OH], a peak of (3385) cm^{-1} was observed. While these peak values moved to (1670 & 1554.05) cm^{-1}, respectively, in the spectrum of Cts-AgTiO_2-5Fu. The stretching vibration of C-F is presumably at (1244) cm^{-1}, according to the 5Fu spectrum. When compared to the spectrum of the Cts-AgTiO_2-5Fu sample, this peak has shifted to (1246.02) cm^{-1}. The 5Fu molecule may have a charge that is positive and hydrogen bonds with the carboxyl bonds even though the fact that both of the protonated groups of amides were almost ionized to create a hydrogen bond. It's possible that the 5Fu molecules and the Cts structure were conjugated. Due to an efficient confinement drug's effective containment inside the polysaccharide combinations, the FTIR spectrum of Cts- Ag-TiO_2-5Fu showed only a few peaks attributable to the drug (Yusefi *et al*., 2021).

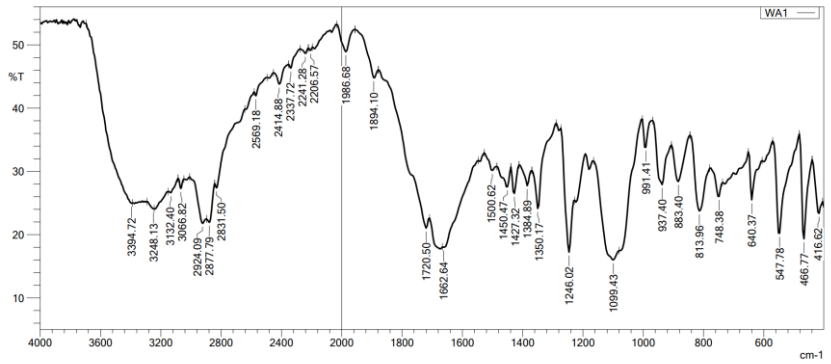
WA1
%T
cm-1
3394.72
3248.13
3132.40
3066.82
2924.09
2877.79
2831.50
2569.18
2414.88
2337.72
2241.28
2206.57
1986.68
1894.10
1720.50
1662.64
1500.62
1450.47
1427.32
1384.89
1350.17
1246.02
1099.43
991.41
937.40
883.40
813.96
748.38
640.37
547.78
466.77
416.62

(a)

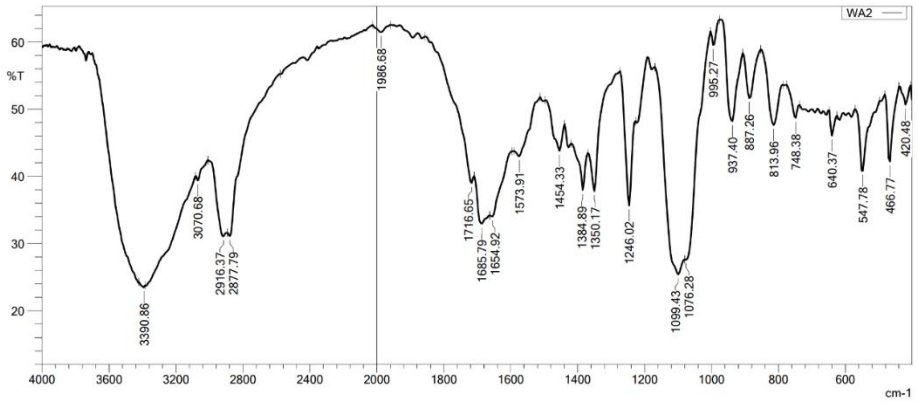
WA2
%T
cm-1
3390.86
3070.68
2916.37
2877.79
1986.68
1716.65
1685.79
1654.92
1573.91
1454.33
1384.89
1350.17
1246.02
1099.43
1076.28
995.27
937.40
887.26
813.96
748.38
640.37
547.78
466.77
420.48

(b)

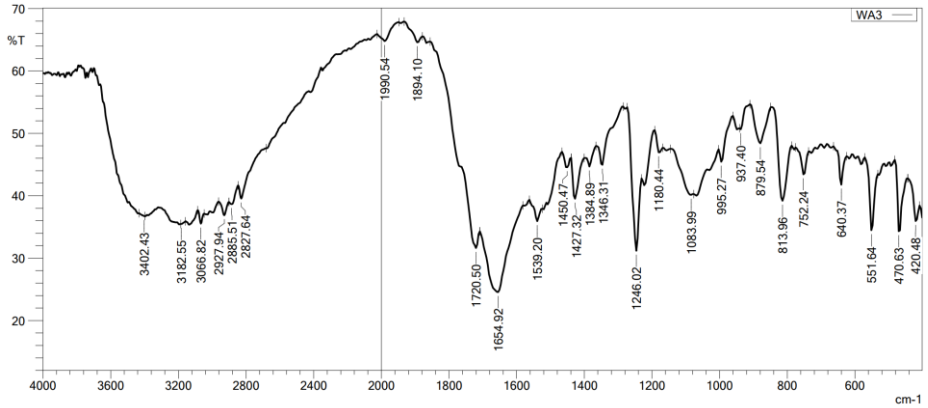
WA3
%T
cm-1
3402.43
3182.55
3066.82
2927.94
2885.51
2827.64
1990.54
1894.10
1720.50
1654.92
1539.20
1450.47
1427.32
1384.89
1346.31
1246.02
1180.44
1083.99
995.27
937.40
879.54
813.96
752.24
640.37
551.64
470.63
420.48

(c)

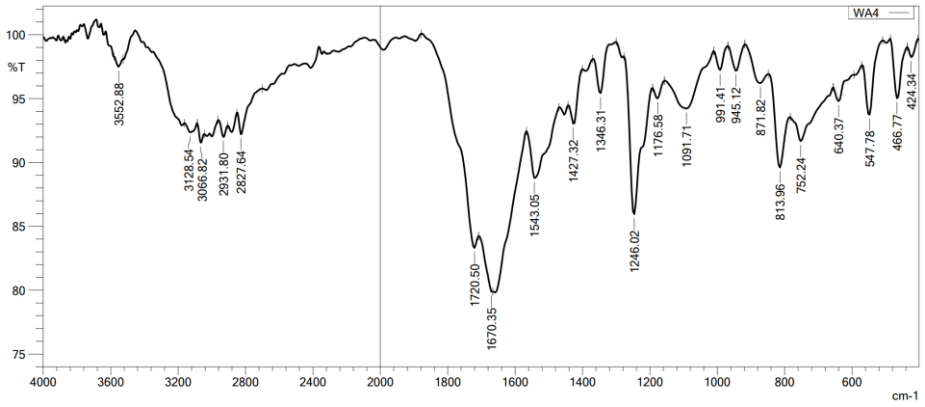

(d)

Figure 3. FTIR spectra of the Synthesized nanocomposites (a) Ag-TiO2-PEG-5Fu, (b) TiO_2-PEG-Fu (unpublished data), (c) 2Ag -TiO_2-PEG-5Fu and (d) Ag-TiO_2-Chitosan-5Fu

5.3. Transmission electron microscopy (TEM) Analysis

The measurement of Ag-TiO_2-PEG-5Fu showed the presence of almost regular spherical structures [11] and these structures were of different sizes, some of which were large (80-100) nm and others small (10-50) nm, the large particles are attributed to TiO_2 and the small ones to silver nanoparticles. It was proved that the large particles of TiO_2 shown in Figure (4b) contain only TiO_2 are identical to the sizes of large spheres in the compound Figure (4a). It was proved that TiO_2 particles in the Ag-TiO_2-PEG-5Fu compound and that in the pure TiO_2 sample have identical size. The samples composition showed in Figure (4c) is similar to that showed in Figure (4a), but the ratio of Ag is twice than of TiO_2. It is shown that more agglomeration of nanoparticles than that appeared in Figure (4a). It was observed that there were chain nanostructures in two colors, one of which is pale and the other is dark. The Pale color can be attributed to TiO_2 and the dark one is to Ag, there is a weak overlapping with each other, with sizes ranging from 30 nm to 100 nm due to aggregation. It can be proved that adding silver in higher ratios can cause change in the structural properties of the composite due to the particle's aggregation which may negatively affect the efficiency of carrying the drugs because in medical applications a wall separated is usually required. Figure (4d) which show the TEM of Ag-TiO_2-Chitosan-5Fu there is aggregation of nanoparticles together and this may be related to the existence of chitosan.

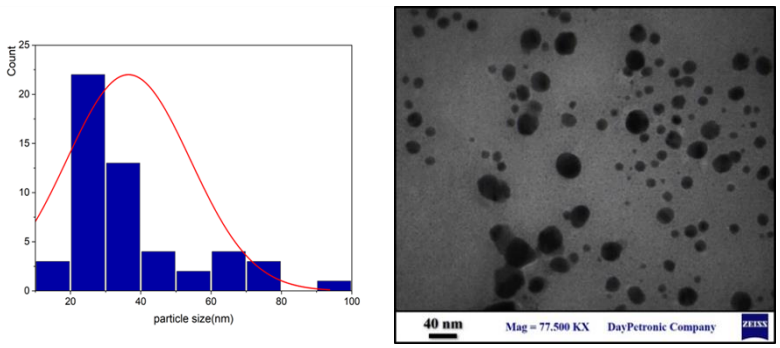

(a)

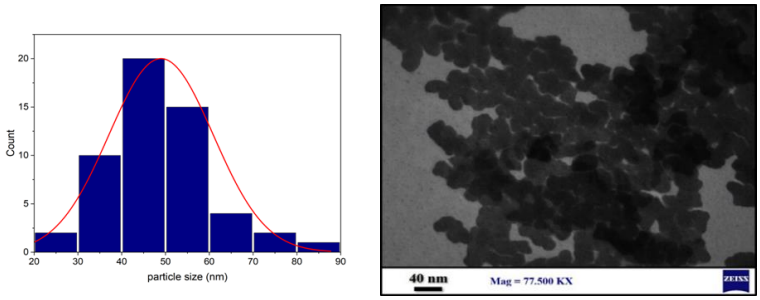

(b)

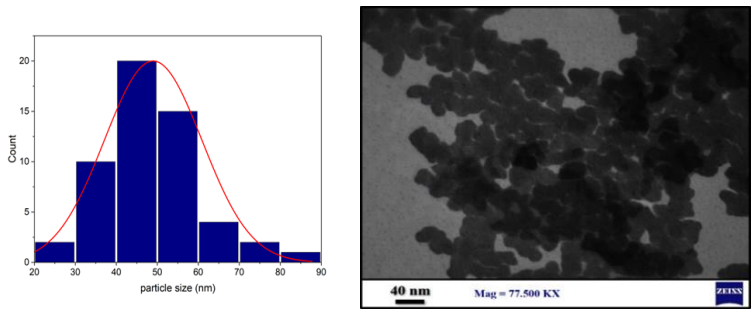

(c)

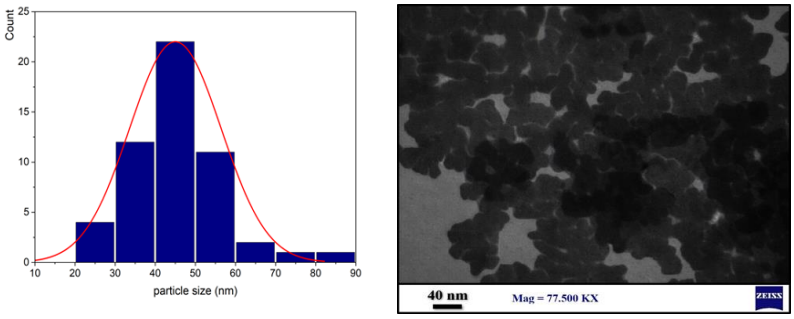

(d)

Figure 4. Transmission electron microscopy images and particle size distribution of (a) $AgTiO_2$ -PEG-5Fu nanocomposite, (b) TiO_2-PEG-5Fu nanocomposite, (c) (2Ag) TiO_2-PEG-5Fu nanocomposite and (d) $AgTiO_2$- Chitosan -5Fu nanocomposite

5.4. X-ray Diffraction (XRD) analysis

The XRD patterns of synthesized $AgTiO_2$ Chitosan 5-Fu and $AgTiO_2$ PEG 5-Fu are shown in (Figure 5a). Peaks of well-defined refraction with 2θ of $AgTiO_2$ Chitosan 5-Fu XRD are at approximately 25° and 28.8°, where the crystal size of the material was determined depending on Scherrer's equation to be 28.90 nm, while $AgTiO_2$ PEG 5-Fu XRD shows that Peaks were at 2θ equals to 25.3°, 27.8°, 28.8° and 31.5°.The crystal size of the material was determined based on Scherrer's equation to be 38.47 nm. It is noticeable that there are several peaks corresponding to each other's between the two composites. Comparing to the previous studies that revealed that the strongest peak of TiO_2 was at 25° and 48° corresponding to (101) and (200) (Antić *et al.*, 2012; Theivasanthi & Alagar, 2013), Ag peaks were observed at 2θ equals to 27.81°, 32.16°,

38.12°, 44.3°, 46.21°, 54.83°, 57.39°, 64.42° and 77.45° corresponding to (210), (122), (111), (200), (231), (142), (241), (220) and (311) (Lalsangpuii *et al*., 2022). The main signals feature in the diffraction line of 5-FU occur as a very intense peak at 2θ equals to 28.7° corresponds to (214) and a much weaker one at 2θ equals to 7° corresponds to (001) , due to the very high intensity of the peak recorded at 2θ equals to 28.7° (Lin *et al*., 2002; Moisescu-goia *et al*., 2017; Nivethaa *et al*., 2016) and for PEG were at 19.5°, 24° and 33.3°corresponding to (120) (032) and (311) (Li *et al*., 2020; Park *et al*., 2008; Song *et al*., 2008). The important XRD characteristic peaks of chitosan are present at 10° and 20° corresponding to (020) and (110) respectively (Hai & Sugimoto, 2018; Venkatesan *et al*., 2017). It can be found that there is a minor difference in the observation of the strongest peaks between this research and prior investigations of pure materials, which could be attributed to material linking.

The XRD pattern of synthesized TiO_2 PEG 5-Fu and $AgTiO_2$ PEG 5-Fu showed in (Figure 5b), the diffraction peaks of TiO_2 PEG 5-Fu at 2θ equals to 20°, 25.3°, 28.8°, 31.5°, 32.3° and 38°. The crystallinity of the material was determined depending on Scherrer's equation to be 42.97 nm. The data of $AgTiO_2$ PEG 5-Fu discussed above comparing both of composite shows that there is an identical peak of 2θ quals 28.8° which is the sharpest peak that explains more structure's crystallinity. The clear difference between two curves is in the presence of peaks at 27.8°and 32.3° that are related to Ag.

Figure 5c shows the XRD pattern of synthesized $AgTiO_2$ PEG 5-FU and $2Ag\ TiO_2$ PEG 5-Fu. $2AgTiO_2$ PEG 5-Fu illustrates peaks at 2θ equals to 20°, 25.3°, 27.8°, 28.8°, 32.3°, 48.3° and 59.3°. The crystal size of the material was determined based on Scherrer's equation to be 37.46 nm. Additionally, $AgTiO_2$ PEG 5-FU patterns are explained above. It's clear that the XRD pattern of synthesized $AgTiO_2$ PEG 5-Fu is sharpest than the XRD pattern of synthesized $2AgTiO_2$ PEG 5-Fu with a very small difference in the crystal size. All composite sharpest peak at 2θ equals to 28.8° are related to 5-FU.

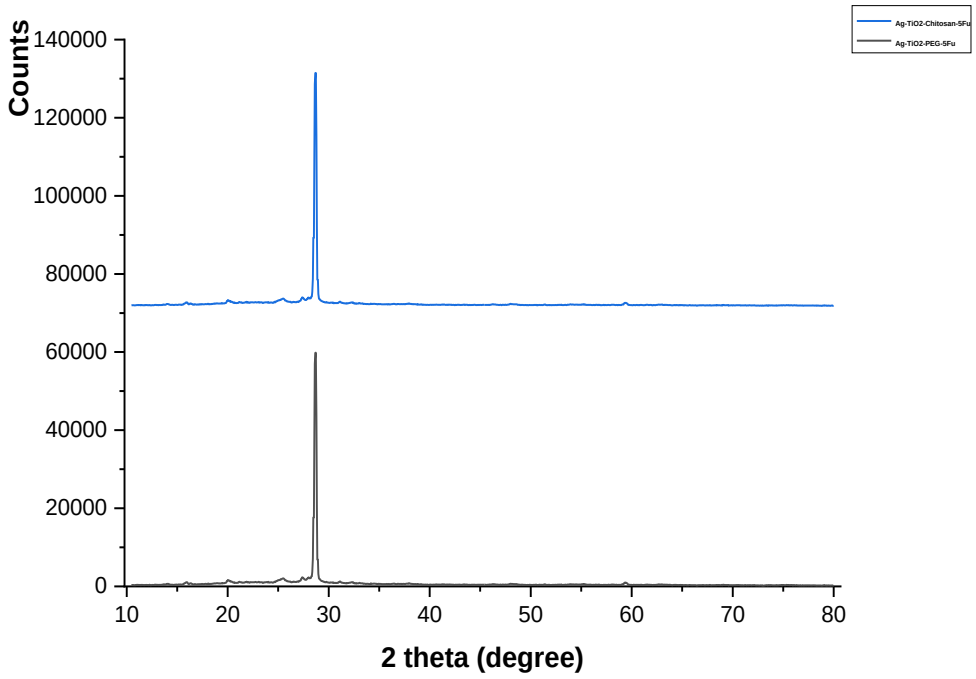

(a)

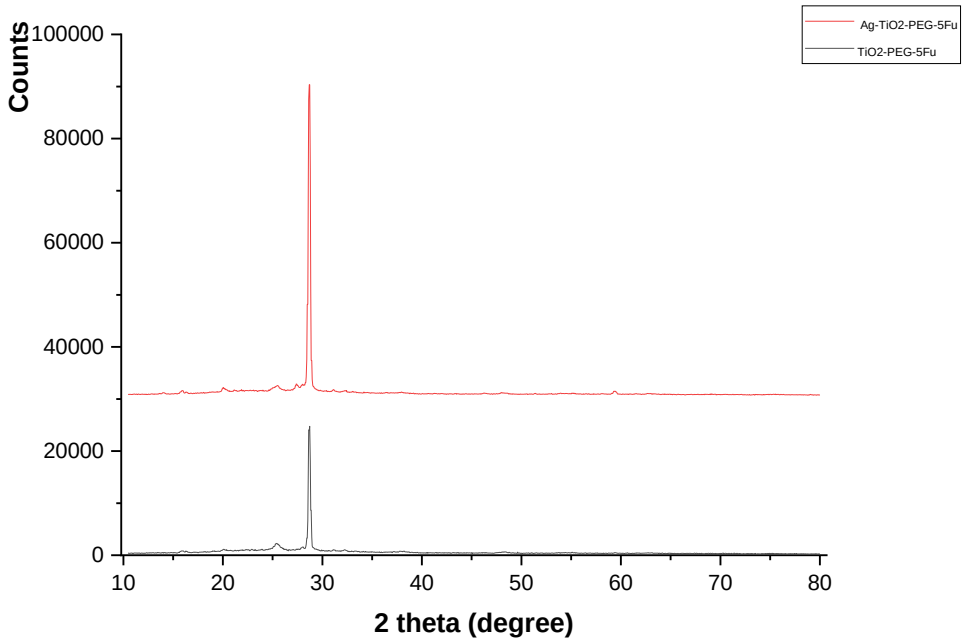

(b)

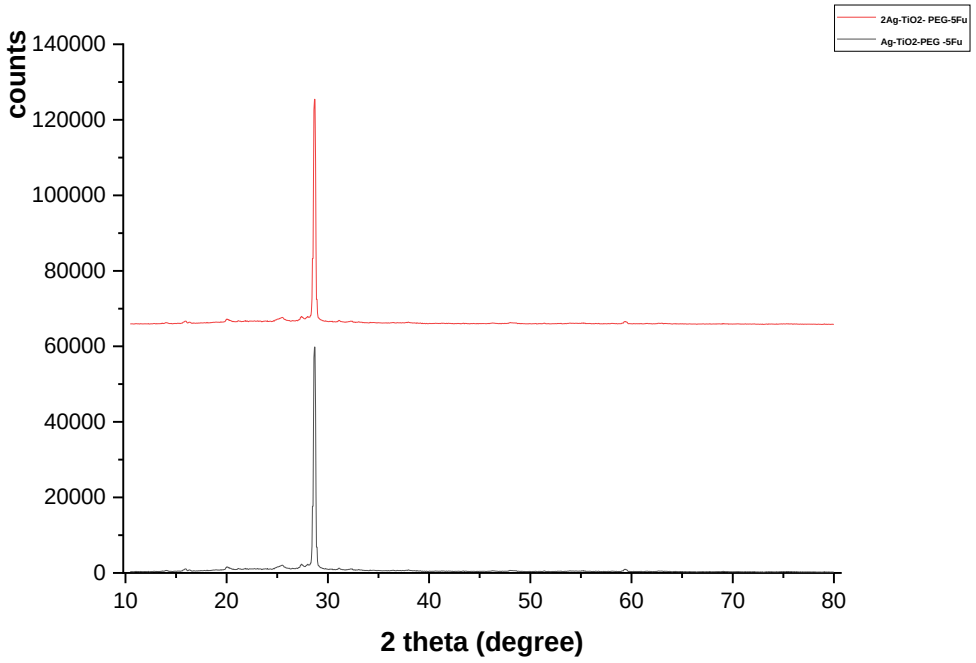

(c)

Figure 5. XRD patterns of (a) [Ag-TiO_2-Chitosan-5Fu] and [Ag-TiO_2-PEG-5Fu], (b) [TiO_2 -PEG -5Fu] and [Ag-TiO_2-PEG-5Fu], (c) [Ag-TiO_2-PEG -5Fu] and [2Ag-TiO_2-PEG-5Fu]

5.5. Optical density of samples- treated nanocomposites

Optical density (OD) is a spectrophotometric measurement that quantifies the amount of light absorbed by a substance. The optical density is used to evaluate the

metabolic activity or viability of cells in the passage describing the MTT test method. In this test, measuring OD yields a value that indicates how many formazan crystals produced in each microplate well. When MTT is broken down by live cells, formazan crystals develop. The greater the number of formazan crystals, the greater the metabolic activity of the cells, indicating that the cells are still alive (Meyers *et al*., 2018).

The liquid nanocomposites were diluted to make serial dilutions of different concentrations (100 µg/ml, 50 µg/ml, 25 µg/ml, 12.5 µg/ml, 6.2 µg/ml and 3.1 µg/ml) for studying their effectiveness on the AMN3 cell line. OD was measured using ELISA and compared to a control group that did not receive treatment. Figure 6a illustrates the results obtained after applying $AgTiO_2$ PEG 5-FU. The statistical analysis using one-way ANOVA indicated a high level of significancy ($p<0.0001$). Tukey's multiple comparisons test revealed a statistically significant difference (at 95% confidence interval (CI)) between the mean optical density of 100 µg/ml which was 0.40 and that of the control (0.90). Similarly, the mean optical densities of 50 µg/ml, 12.5 µg/ml, 25 µg/ml and 6.25 µg/ml showed statistically significant decrease (at 95% CI) when compared to that of the control, where their densities were 0.52, 0.65, 0.74 and 0.80, respectively. However at the concentration of 3.1 µg/ml, there was no significant difference between the mean optical densities when compared to the control. Zakaria et al. (2013) also tested different concentrations of aqueous crude extract on AMN3 cell line and found that increasing the concentration led to reduction in cell viability (Meyers *et al*., 2018).

The mean optical density of samples treated with TiO_2 PEG 5-FU nanocomposites shown in Figure 6b at different concentrations (100 µg/ml, 50 µg/ml, 25 µg/ml, 12.5 µg/ml, 6.25 µg/ml and 3.1 µg/ml) exhibited statistically significant decrease (at 95% CI) when comparing their optical densities with that of control (had an optical density of 0.81). Specifically, 100 µg/ml had an optical density of 0.40, while the optical densities of 50 µg/ml, 25 µg/ml, 12.5 µg/ml, 6.25 µg/ml and 3.1 µg/ml were (0.49), (0.54), (0.58), (0.66) and (0.75) respectively. Significantly, statistical differences in the mean optical density of samples treated with $2AgTiO_2$ PEG 5-FU were observed as shown in Figure 6c, among the various concentrations when compared to the control optical density (0.85). The concentration of 100 µg/ml exhibited a statistically significant decrease (at 95% CI) with a mean optical density of 0.45. Similarly, the concentrations of 50 µg/ml (mean OD was 0.52), 25 µg/ml (mean OD was 0.67), 12.5 µg/ml (mean OD was 0.72) and 6.25 µg/ml (mean OD was 0.79) all showed statistically significant differences (at 95% CI) with lower values compared to the control. In contrast, the concentration of 3.1 µg/ml (mean OD was 0.82) did not exhibit any significant difference when compared to the control, suggesting that there was no notable impact on the optical density compared to the control. Overall, these results indicate a clear trend of decrease in the mean optical density as the concentration of the nanocomposites increase with statistically significant differences observed for the higher concentrations of 100 µg/ml, 50 µg/ml, 25 µg/ml, 12.5 µg/ml and 6.25 µg/ml when compared to the control. In Figure 6d, samples treated with $AgTiO_2$ Chitosan 5-FU also showed a clear trend of decrease in the mean optical density when compared the various concentrations (100 µg/ml, 50 µg/ml, 25 µg/ml, 12.5 µg/ml, 6.25 µg/ml and 3.1 µg/ml) to the control value of 0.90. The concentration of 100 µg/ml showed a statistically significant difference (at 95% CI) with a mean OD of 0.41, which was significantly lower than that of the control (0.90). Similarly, the concentration of 50 µg/ml exhibited a statistically significant difference (at 95% CI) with a mean OD of 0.43. The mean optical densities of 25 µg/ml, 12.5 µg/ml, 6.25 µg/ml and 3.1 µg/ml were also significantly lower than that of the control, where there were 0.54, 0.57, 0.72

and 0.82, respectively. These findings suggest that as the concentration of the nanocomposites decreases, the mean optical density increase and this trend is statistically significant.

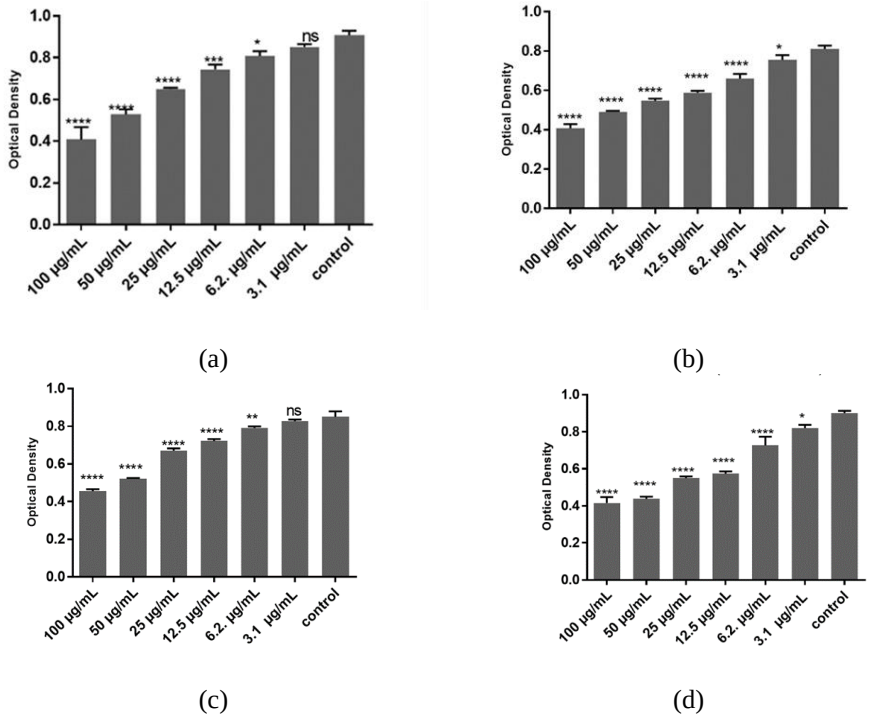

Figure 6. Influence of (a) $AgTiO_2$ PEG 5-FU; (b) TiO_2 PEG 5-FU; (c) $2AgTiO_2$ PEG 5-FU and (d) $AgTiO_2$ Chitosan 5-FU after incubation of 72 h. Statistical significance analyzed with one-way ANOVA different levels: * $p < 0.05$, ** $p < 0.01$, *** $p < 0.001$ and **** $p < 0.0001$. All results are presented as mean± SD of triplicate measurements

5.6. Cytotoxicity of samples- treated nanocomposites

The cytotoxic effect exposure to various concentrations of different nanocomposites after 72hr on AMN3 cell line is shown in Table 1.

Table 1. Cytotoxic effect exposure to various concentrations of different nanocomposites after 72hr on AMN3 cell line

Conc. of Nano. µg/ml	Cytotoxicity of Nanocomposite %						
	5-FU	chitosan	PEG	$AgTiO_2$ PEG 5-FU	$2AgTiO_2$ PEG 5-FU	TiO_2 PEG 5-FU	$AgTiO_2$ Chitosan 5-FU
100	60.8	45.3	20.9	55.0	46.3	49.7	53.8
50	36.4	41.5	20.5	32.6	38.8	39.3	51.4
25	22.8	35.2	19.1	28.4	21.0	32.5	39.0
12.5	19.6	28.8	9.7	17.9	15.1	27.2	36.2
6.2	11.7	16.6	0.8	10.9	6.9	18.5	19.2
3.1	2.2	8.2	0	6.1	2.7	6.9	8.8

5.6.1. Nanocomposite effectiveness

To study the nanocomposites effectiveness, the cytotoxic effect of different composites loaded with5-FU are compared with that of 5-FU itself. All samples

developed by the laser ablation process, which has various advantages for nanoparticle synthesis and drug delivery, including precision, green synthesis, high purity, adaptability and drug loading compatibility at the desired concentrations. These advantages make laser ablation an appealing method for creating new drug delivery systems that improve treatment outcomes. The results show that the inhibition rates of 5-FU are usually higher when it is used in pure form than when it is mixed with other materials to make composites. This difference is noticeable across different doses.

In the case of pure 5-FU, the rates of inhibition are 60.8%, 36.4%, 22.8%, 19.6%, 11.7% and 2.2% at concentration of 100 μg/ml, 50 μg/ml, 25 μg/ml, 12.5 μg/ml, 6.2 μg/ml and 3.1 μg/ml, respectively. Compared to these rates, the inhibition rates of the composites that contain 5-FU seem to be reliably lower. This is especially true for $AgTiO_2$ PEG 5-FU and $AgTiO_2$ Chitosan 5-FU. Considering $AgTiO_2$ PEG 5-FU composite as an example, at a concentration of 100 g/ml, the highest rate of cytotoxicity was found to be 55% and the other serial dilution were 32.6%, 28.4%,17.9%,10.9% and 6.1%, which is lower than the rate of inhibition seen at the same concentration of 100 g/ml for pure 5-FU (60.8%). Other composite formulations, like $AgTiO_2$ Chitosan 5-FU with cytotoxicity of (53.8%, 51.40%, 39.0%, 36.2%, 19.2% and 8.8%) for the same serial dilutions, show a similar pattern. The lower inhibition rates observed in mixed forms compared to pure 5-FU do not necessarily indicate that the therapy is less effective. Rather, these lower diminution rates may indicate that the drug has a smaller impact on healthy cells while maintaining a certain level of cytotoxicity against cancer cells. Importantly, the composite formulations maintain a stable equilibrium with a 1:1:1:1 ratio of Ag:TiO_2:polymer:5-FU components. This information demonstrates how it may be possible to develop novel therapeutic models by utilizing the composite's ability to fine-tune the effect of the substance. This could alter the delicate equilibrium between cancer treatment efficacy and safety. It noticeable for nanocomposite of $AgTiO_2$ Chitosan 5-FU at the concentration of 50 g/ml, 25 g/ml, 12.5 g/ml, 6.2 g/ml and 3.1 g/ml have higher cytotoxic effect than 5-FU itself which may be related to the anticancer activity of chitosan. The changes in morphology of cell compared with control (not-treated cells) are shown in Figure 7.

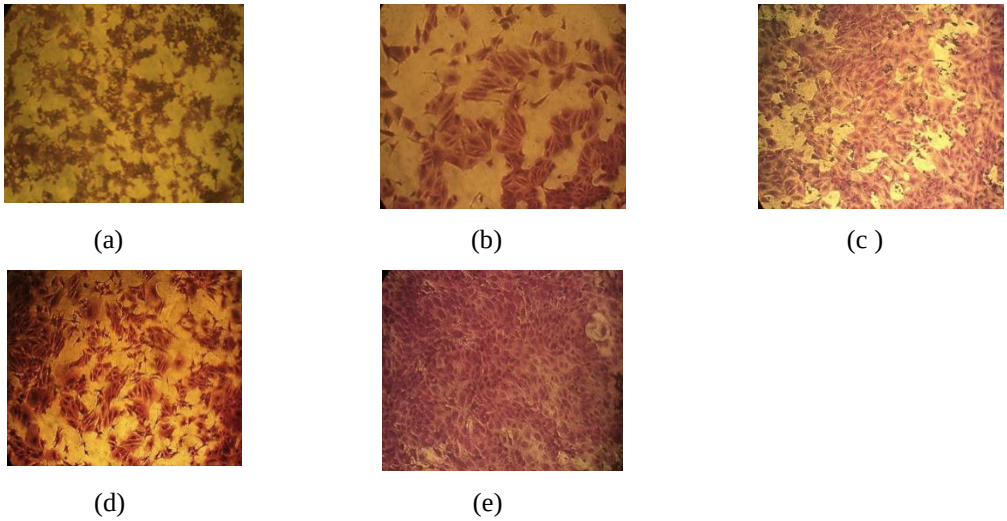

Figure 7. Changes in Cell Morphology after applying (a) $AgTiO_2$ PEG 5-Fu, (b) TiO_2 PEG 5-FU; (c) $2AgTiO_2$ PEG 5-Fu, (d) $AgTiO_2$ chitosan and (e) not treated AMN3 cell line. The magnification power is 200X

5.6.2. The effectiveness of doubling Ag concentration on the spread of drug loaded nanocomposite.

The decrease in cytotoxicity observed in the case of ($2AgTiO_2$ PEG 5-FU) shown in table ….. can be attributed to the phenomenon of agglomeration, as evidenced by the TEM (section 5.3). Agglomeration refers to the clustering or aggregation of nanoparticles, resulting in the formation of larger particle assemblies. In this case, the increased concentration of Ag is likely responsible for the observed agglomeration. This agglomeration of nanoparticles can have significant implications for their biological activity. When nanoparticles agglomerate, their physical and chemical properties can be altered, including their surface area, surface chemistry and the availability of active sites for interaction with biological systems (Zhang, 2014). In the context of ($2AgTiO_2$ PEG 5-FU), the increased Ag concentration likely leads to stronger interparticle interactions, It demonstrated agglomeration by comparing with $AgTiO_2$PEG5-FU composite that exhibited cytotoxicity of (55%, 32.60%, 28.4%, 17.9%, 10.9% and 6.1%), while $2AgTiO_2$ PEG 5-FU exhibited cytotoxicity of (46.3%, 38.8%, 21.0%, 15.1%, 6.9% and 2.7%) for the same serial dilutions. The agglomerated nanoparticles may have reduced surface area compared to individual, dispersed nanoparticles, which can limit their interaction with target cells or tissues (Mahmoudi *et al*., 2011). The decrease in cytotoxicity observed in ($2AgTiO_2$ PEG 5-FU) can be explained by the reduced effectiveness of agglomerated nanoparticles in interacting with cancer cells. The decreased surface area of agglomerated nanoparticles may hinder their ability to come into contact with cancer cells, limiting their potential to exert cytotoxic effects (Ashraf *et al*., 2018). It is important to note that the agglomeration phenomenon can be influenced by various factors, including particle concentration, size and surface chemistry (Jiang *et al*., 2009). In the case of ($2AgTiO_2$ PEG 5-FU), the higher Ag concentration likely promotes stronger particle interactions, leading to agglomeration. Agglomeration can impact the overall behavior and biological activity of the nanoparticles, including their cytotoxicity. To enhance the cytotoxicity and therapeutic efficacy of ($2AgTiO_2$ PEG 5-FU) and similar nanoparticle formulations, strategies to mitigate agglomeration should be explored. In contrast, the study of P.C. Nagajyothi et al. (2021) found that ZnO/Ag nanocomposites with the optimal Ag concentration could be a potential candidate for biomedical applications and Hariharan et al. (2020) which showed that increasing the Ag content led to an increase anticancer activity. The changes in morphology of cell compared with control (not-treated cells) are shown in Figure 8.

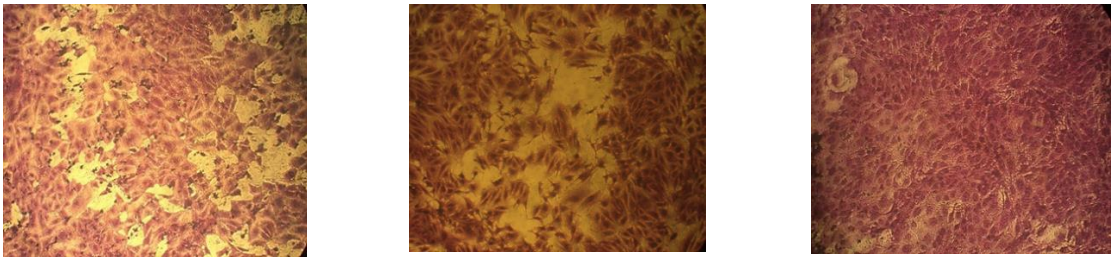

(a) (b) (c)

Figure 8. Changes in Cell Morphology after applying (a) $AgTiO_2$ PEG 5-Fu, (b) $2AgTiO_2$ PEG and (c) not treated AMN3 cell line. The magnification power is 200X

5.6.3. $AgTiO_2$ PEG 5-FU vs TiO_2 PEG 5-FU effectiveness

The composite of $AgTiO_2$ PEG with 5-fluorouracil (5-FU) demonstrated noteworthy cytotoxic effects on the AMN3 cell line following a 72-hour exposure. The highest concentration of 100 µg/ml exhibited the most significant inhibition rate, reaching 55%. This high rate indicates a substantial level of cytotoxicity induced by the composite. Subsequently, the concentrations of 50 µg/ml, 25 µg/ml, 12.5 µg/ml, 6.2 µg/ml and 3.1 µg/ml displayed inhibition rates of 32.60%, 28.4%, 17.9%, 10.9% and 6.1%, respectively. In comparison, the TiO_2 PEG 5-FU composite exhibited inhibition rates for the mentioned concentrations as follows: 49.7%, 39.30%, 32.5%, 27.2%, 18.5% and 6.9%. It is evident that the TiO_2 PEG 5-FU composite generally demonstrated higher inhibition rates compared to the $AgTiO_2$ PEG 5-FU composite at equivalent concentrations. The results agrees with Byeon et al. (2016) who said that despite the fact that Ag-TiO_2 nanoparticles released the metallic component to obviously contribute to cytotoxicity, the released fraction of the PEG-incorporated particles was not significantly affected due to the biocompatible organic coating PEG which is employed as overlayers for the Ag-TiO_2 nanoparticles. The observed lower inhibition rates of $AgTiO_2$ PEG compared to TiO_2 PEG indicate that the biocompatible PEG coating successfully maintained the stability and reduced the cytotoxic potential of the released metallic component. Azimee et al. (2020) showed that the amalgamation of TiO_2 nanoparticles (NPs) with 5-fluorouracil (5-FU) enhanced the cytotoxic and apoptotic effects of chemotherapy in AGS gastric cancer cells by inhibiting autophagy. Based on these findings, it can be concluded that the composite of $AgTiO_2$ PEG with 5-FU exhibited cytotoxic effects on the AMN3 cell line, albeit with slightly lower inhibition rates compared to that of TiO_2 PEG 5-FU composite.

6. Conclusions

It can be evident from the study that by adding the polymers to the composite, the blue shift had already occurred, indicating that the NPs were effectively formed and the size of the particles had decreased. It is clear that doubling the Ag concentration leads to particles aggregation. Thus, adding silver at higher rate is not suitable in some medical applications, especially in drug delivery application. It is noticed that a very small shift of peaks in the prepared composites observed in the XRD compared to the original peaks of the pure chemicals in previous studies and this could be referred to the linking between materials in the final product and the more crystalline composite is Ag-TiO_2-PEG-5Fu with the sharpest peak at 2θ equals 28.8°. In sum, blending polymers with nanometals significantly improved the properties of the nanoparticles. These nanocomposites are promising to be used in drug delivery applications. The incorporation of polymers and 5-fluorouracil (5-Fu) significantly enhanced the cytotoxic effects of these composite materials, indicating their potential for use in the targeted delivery of anticancer medications. The results of the investigation indicate that the $AgTiO_2$ PEG 5-Fu exhibited notable cytotoxicity, displaying the maximum efficacy at a concentration of 100 g/ml, resulting in an inhibition rate of 55%. The comparative cytotoxicity of two different composites, namely $AgTiO_2$ PEG 5-Fu and $AgTiO_2$ Chitosan 5-Fu, was observed to be comparable. Interestingly, it was shown that increasing the concentration of silver (Ag) in $AgTiO_2$ PEG 5-Fu led to a reduction in cytotoxicity, potentially attributable to the aggregation of Ag particles. The observed nanocomposites demonstrate an increased level of cytotoxicity and inhibition towards cancer cells, establishing them as potential contenders for targeted drug delivery applications. Additional in vivo studies and further

optimization are necessary in order to fully exploit the potential of these nanocomposites for medical purposes. The potential of these nanomaterial composites in mitigating the adverse effects of 5-FU on healthy tissues is significant.

References

Al-Amin, M., Dey, S.C., Rashid, T.U., Ashaduzzaman, M. & Shamsuddin, S.M. (2016). Solar assisted photocatalytic degradation of reactive azo dyes in presence of anatase titanium dioxide. *Int. J. Latest Res. Eng. Technol*, *2*(3), 14-21.

Al-Salman, H.N.K., Ali, E.T., Jabir, M., Sulaiman, G.M. & Al-Jadaan, S.A. (2020). 2-Benzhydrylsulfinyl-N-hydroxyacetamide-Na extracted from fig as a novel cytotoxic and apoptosis inducer in SKOV-3 and AMJ-13 cell lines via P53 and caspase-8 pathway. *European Food Research and Technology*, 246, 1591-1608.

Al-Shammari, A.M., Al-Saadi, H., Al-Shammari, S.M. & Jabir, M.S. (2020, March). Galangin enhances gold nanoparticles as anti-tumor agents against ovarian cancer cells. In *AIP Conference Proceedings*, *2213*(1). AIP Publishing.

Al-Ziaydi, A.G., Al-Shammari, A.M., Hamzah, M.I. & Jabir, M.S. (2020). Hexokinase inhibition using D-Mannoheptulose enhances oncolytic newcastle disease virus-mediated killing of breast cancer cells. *Cancer Cell International*, *20*(1), 1-10.

Al-Ziaydi, A.G., Al-Shammari, A.M., Hamzah, M.I., Kadhim, H.S. & Jabir, M.S. (2020). Newcastle disease virus suppress glycolysis pathway and induce breast cancer cells death. *Virusdisease*, 31, 341-348.

Al-Ziaydi, A.G., Hamzah, M.I., Al-Shammari, A.M., Kadhim, H.S. & Jabir, M.S. (2020, December). The anti-proliferative activity of D-mannoheptulose against breast cancer cell line through glycolysis inhibition. In *AIP Conference Proceedings, 2307*(1). AIP Publishing.

Anirudhan, T.S., Nima, J. & Divya, P.L. (2015). Synthesis, characterization and in vitro cytotoxicity analysis of a novel cellulose based drug carrier for the controlled delivery of 5-fluorouracil, an anticancer drug. *Applied Surface Science*, 355, 64-73.

Antić, Ž., Krsmanović, R.M., Nikolić, M.G., Marinović-Cincović, M., Mitrić, M., Polizzi, S. & Dramićanin, M.D. (2012). Multisite luminescence of rare earth doped TiO_2 anatase nanoparticles. *Materials Chemistry and Physics, 135*(2-3), 1064-1069.

Ashraf, M.A., Peng, W., Zare, Y. & Rhee, K.Y. (2018). Effects of size and aggregation/agglomeration of nanoparticles on the interfacial/interphase properties and tensile strength of polymer nanocomposites. *Nanoscale Research Letters*, 13, 1-7.

Azimee, S., Rahmati, M., Fahimi, H. & Moosavi, M.A. (2020). TiO_2 nanoparticles enhance the chemotherapeutic effects of 5-fluorouracil in human AGS gastric cancer cells via autophagy blockade. *Life Sciences*, 248, 117466.

Bahjat, H.H., Ismail, R.A., Sulaiman, G.M. & Jabir, M.S. (2021). Magnetic field-assisted laser ablation of titanium dioxide nanoparticles in water for anti-bacterial applications. *Journal of Inorganic and Organometallic Polymers and Materials*, 31, 3649-3656.

Barreca, F., Acacia, N., Barletta, E., Spadaro, D., Curro, G. & Neri, F. (2010). Small size TiO_2 nanoparticles prepared by laser ablation in water. *Applied Surface Science, 256*(21), 6408-6412.

Boutinguiza, M., Comesaña, R., Lusquiños, F., Riveiro, A., Del Val, J. & Pou, J. (2015). Production of silver nanoparticles by laser ablation in open air. *Applied Surface Science*, 336, 108-111.

Byeon, J.H. (2016). Scalable hybrid chemical manufacture to photothermal therapy: PEG-capped phototransducers. *Scientific Reports, 6*(1), 31351.

Cuenya, B.R. (2010). Synthesis and catalytic properties of metal nanoparticles: Size, shape, support, composition and oxidation state effects. *Thin Solid Films, 518*(12), 3127-3150.

Fahmy, A., Al-Zomarawy, A., Sayed, A.Z., El-Arab, M.A.E., Shehata, H.A. & Saeed, A.M. (2015). Silver/polyethylene glycol nanocomposite thin films and its biological applications. *Journal of Advances in Chemistry, 11*(5).

Fernández-Arias, M., Zimbone, M., Boutinguiza, M., Del Val, J., Riveiro, A., Privitera, V., Grimaldi, M.G., & Pou, J. (2019). Synthesis and deposition of Ag nanoparticles by combining laser ablation and electrophoretic deposition techniques. *Coatings, 9*(9), 571.

Hai, T.A.P., Sugimoto, R. (2018). Fluorescence control of chitin and chitosan fabricated via surface functionalization using direct oxidative polymerization. *RSC Advances, 8(*13), 7005-7013.

Hariharan, D., Thangamuniyandi, P., Christy, A.J., Vasantharaja, R., Selvakumar, P., Sagadevan, S., Pugazhendhi, A. & Nehru, L. (2020). Enhanced photocatalysis and anticancer activity of green hydrothermal synthesized Ag@ TiO_2 nanoparticles. *Journal of Photochemistry and Photobiology B: Biology*, 202, 111636.

Herbani, Y., Nasution, R., Mujtahid, F. & Masse, S. (2018). Pulse laser ablation of Au, Ag and Cu metal targets in liquid for nanoparticle production. *Journal of Physics: Conference Series, 985*(1), 012005. IOP Publishing.

Jabir, M.S., Sulaiman, G.M., Taqi, Z.J. & Li, D. (2017). Iraqi propolis increases degradation of IL-1β and NLRC4 by autophagy following Pseudomonas aeruginosa infection. *Microbes and Infection*, *20*(2), 89-100.

Jiang, J., Oberdörster, G. & Biswas, P. (2009). Characterization of size, surface charge and agglomeration state of nanoparticle dispersions for toxicological studies. *Journal of Nanoparticle Research*, 11, 77-89.

Khashan, K.S., Sulaiman, G.M., Abdulameer, F.A., Albukhaty, S., Ibrahem, M.A., Al-Muhimeed, T. & AlObaid, A.A. (2021). Antibacterial activity of TiO_2 nanoparticles prepared by one-step laser ablation in liquid. *Applied Sciences, 11*(10), 4623.

Kong, F.Y., Zhang, J.W., Li, R.F., Wang, Z.X., Wang, W.J. & Wang, W. (2017). Unique roles of gold nanoparticles in drug delivery, targeting and imaging applications. *Molecules, 22*(9), 1445.

Kumar, C.S. (2013). *UV-VIS and Photoluminescence Spectroscopy for Nanomaterials Characterization*, 111. Berlin: Springer.

Lalsangpuii, F., Rokhum, S.L., Nghakliana, F., Fakawmi, L., Ruatpuia, J.V., Laltlanmawii, E., Lalfakzuala, R. & Siama, Z. (2022). Green synthesis of silver nanoparticles using spilanthes acmella leaf extract and its antioxidant-mediated ameliorative activity against doxorubicin-induced toxicity in Dalton's Lymphoma Ascites (DLA)-bearing mice. *ACS Omega, 7*(48), 44346-44359.

Li, R., Wu, Y., Bai, Z., Guo, J. & Chen, X. (2020). Effect of molecular weight of polyethylene glycol on crystallization behaviors, thermal properties and tensile performance of polylactic acid stereocomplexes. *RSC Advances, 10*(69), 42120-42127.

Lin, F.H., Lee, Y.H., Jian, C.H., Wong, J.M., Shieh, M.J. & Wang, C.Y. (2002). A study of purified montmorillonite intercalated with 5-fluorouracil as drug carrier. *Biomaterials, 23*(9), 1981-1987.

Maaspuro, M. (2021). Novel ideas for thermal management of filament LED light bulbs. *International Journal of Online and Biomedical Engineering, 17*(8), 60-73.

Mahmoudi, M., Lynch, I., Ejtehadi, M.R., Monopoli, M.P., Bombelli, F.B. & Laurent, S. (2011). Protein - nanoparticle interactions: Opportunities and challenges. *Chemical Reviews*, *111*(9), 5610-5637.

Mathew, L., Chandrasekaran, N. & Mukherjee, A. (2010). Biomimetic synthesis of nanoparticles: science, technology & applicability. *Biomimetics Learning from Nature*.

Merve, O., Şanli, N. & Kondolot Solak, E. (2012). Release of anticancer drug 5 fluorouracil from different ionically crosslinked alginate beads. *Journal of Biomaterials and Nanobiotechnology*, *3*(4).

Messina, G.C. (2013). *In Liquid Laser Processes for Metal Nanoparticles Synthesis and Manipulation.* Università degli Studi di Catania

Meyers, A., Furtmann, C. & Jose, J. (2018). Direct optical density determination of bacterial cultures in microplates for high-throughput screening applications. *Enzyme and Microbial Technology*, 118, 1-5.

Moisescu-goia, C., Muresan-Pop, M. & Simon, V. (2017). XRD checking of crystalline forms resulted by slow evaporation of 5-fluorouracil solutions obtained with different solvents. *Studia Universitatis Babeş-Bolyai Physica*, 15-21.

Nagajyothi, P., Muthuraman, P., Tettey, C., Yoo, K. & Shim, J. (2021). In vitro anticancer activity of eco-friendly synthesized ZnO/Ag nanocomposites. *Ceramics International, 47*(24), 34940-34948.

Narmani, A., Arani, M.A.A., Mohammadnejad, J., Vaziri, A.Z., Solymani, S., Yavari, K., Talebi, F. & Darzi, S.J. (2020). Breast tumor targeting with PAMAM-PEG-5FU-99m Tc as a new therapeutic nanocomplex: In in-vitro and in-vivo studies. *Biomedical Microdevices*, 22, 1-13.

Nazir, S., Khan, M.U.A., Al-Arjan, W.S., Abd Razak, S.I., Javed, A. & Kadir, M.R.A. (2021). Nanocomposite hydrogels for melanoma skin cancer care and treatment: In-vitro drug delivery, drug release kinetics and anti-cancer activities. *Arabian Journal of Chemistry, 14*(5), 103120.

Nivethaa, E., Dhanavel, S., Rebekah, A., Narayanan, V. & Stephen, A. (2016). A comparative study of 5-Fluorouracil release from chitosan/silver and chitosan/silver/MWCNT nanocomposites and their cytotoxicity towards MCF-7. *Materials Science and Engineering: C*, 66, 244-250.

Park, J. Y., Daksha, P., Lee, G. H., Woo, S. & Chang, Y. (2008). Highly water-dispersible PEG surface modified ultra small superparamagnetic iron oxide nanoparticles useful for target-specific biomedical applications. *Nanotechnology, 19*(36), 365603.

Praveen, P., Viruthagiri, G., Mugundan, S. & Shanmugam, N. (2014). Structural, optical and morphological analyses of pristine titanium di-oxide nanoparticles–Synthesized via sol–gel route. *Spectrochimica Acta Part A: Molecular and Biomolecular Spectroscopy*, 117, 622-629.

Qin, J.S., Du, D.Y., Li, W.L., Zhang, J.P., Li, S.L., Su, Z.M., Wang, X.L., Xu, Q., Shao, K.Z., & Lan, Y.Q. (2012). N-rich zeolite-like metal–organic framework with sodalite topology: High CO_2 uptake, selective gas adsorption and efficient drug delivery. *Chemical Science, 3*(6), 2114-2118.

Ramlli, M., Maksud, M. & Isa, M. (2017). Characterization of polyethylene glycol plasticized carboxymethyl cellulose-ammonium fluoride solid biopolymer electrolytes. In *AIP Conference Proceedings, 1826*(1). AIP Publishing.

Roduner, E. (2006). Size matters: Why nanomaterials are different. *Chemical Society Reviews, 35*(7), 583-592.

Safwat, M.A., Soliman, G.M., Sayed, D. & Attia, M.A. (2018). Fluorouracil-loaded gold nanoparticles for the treatment of skin cancer: Development, in vitro characterization and in vivo evaluation in a mouse skin cancer xenograft model. *Molecular Pharmaceutics, 15*(6), 2194-2205.

Sağir, T., Huysal, M., Durmus, Z., Kurt, B.Z., Senel, M. & Isık, S. (2016). Preparation and in vitro evaluation of 5-flourouracil loaded magnetite–zeolite nanocomposite (5-FU-MZNC) for cancer drug delivery applications. *Biomedicine & Pharmacotherapy*, 77, 182-190.

Sasaki, T., Shimizu, Y. & Koshizaki, N. (2006). Preparation of metal oxide-based nanomaterials using nanosecond pulsed laser ablation in liquids. *Journal of Photochemistry and Photobiology A: Chemistry, 182*(3), 335-341.

Semaltianos, N., Logothetidis, S., Perrie, W., Romani, S., Potter, R., Sharp, M., Dearden, G. & Watkins, K. (2009). CdTe nanoparticles synthesized by laser ablation. *Applied physics Letters, 95*(3), 191.

Shukri, W.N.W., Bidin, N., Islam, S. & Krishnan, G. (2018). Synthesis of Au-Ag alloy nanoparticles in deionized water by pulsed laser ablation technique. *Journal of Nanoscience and Nanotechnology*, 18, 1-11.

Škorc, G., Šafarič, R., Lukman, D., Ivanovich Protsenko, S. & Zapusek, S. (2010). Interface between macro and nano worlds. *International Journal of Online Engineering, 6*(1), 52-59.

Song, R., Xue, R., He, L.H., Liu, Y. & Xiao, Q.L. (2008). The structure and properties of chitosan/polyethylene glycol/silica ternary hybrid organic-inorganic films. *Chinese Journal of Polymer Science, 26*(05), 621-630.

Tajdidzadeh, M., Azmi, B.Z., Yunus, W.M.M., Talib, Z.A., Sadrolhosseini, A.R., Karimzadeh, K. & Dorraj, M. (2014). Synthesis of silver nanoparticles dispersed in various aqueous media using laser ablation. *The Scientific World Journal*, 2014.

Theivasanthi, T., Alagar, M. (2013). Titanium dioxide (TiO_2) nanoparticles XRD analyses: An insight. *arXiv preprint arXiv:1307.1091*.

Titov, I. E., Smirnova, O.A., Glotov, A.N. & Golovin, A.D. (2012). Remote Laser Laboratory: lifebuoy for laser engineering curriculum. I*nternational Journal of Online Engineering, 8*(2), 23-27.

Tomoiaga, A.M., Ochiuz, L. & Vasile, A. (2013). Sonochemical development of magnetic nanoporous therapeutic systems as carriers for 5-Fluorouracil. *Journal of Nanotechnology, 1*(1), 27.

Tsuji, T., Iryo, K., Watanabe, N. & Tsuji, M. (2002). Preparation of silver nanoparticles by laser ablation in solution: Influence of laser wavelength on particle size. *Applied Surface Science, 202*(1-2), 80-85.

Venkatasubbu, G.D., Ramasamy, S., Ramakrishnan, V. & Kumar, J. (2013). Folate targeted PEGylated titanium dioxide nanoparticles as a nanocarrier for targeted paclitaxel drug delivery. *Advanced Powder Technology, 24*(6), 947-954.

Venkatesan, J., Lee, J.Y., Kang, D.S., Anil, S., Kim, S.K., Shim, M.S. & Kim, D.G. (2017). Antimicrobial and anticancer activities of porous chitosan-alginate biosynthesized silver nanoparticles. *International Journal of Biological Macromolecules*, 98, 515-525.

Yusefi, M., Chan, H.Y., Teow, S.Y., Kia, P., Lee-Kiun Soon, M., Sidik, N.A.B.C. & Shameli, K. (2021). 5-fluorouracil encapsulated chitosan-cellulose fiber bionanocomposites: Synthesis, characterization and in vitro analysis towards colorectal cancer cells. *Nanomaterials, 11*(7), 1691.

Zakaria, A.S., Hazha, J.H. (2013). Cytogenetic toxicity effects of local purslane (portulaca oleracea) leaf crude extracts on normal and cancer cell lines in vitro. *International Journal of Drug Discovery, 5*(1), 173.

Zeng, H., Du, X.W., Singh, S.C., Kulinich, S.A., Yang, S., He, J. & Cai, W. (2012). Nanomaterials via laser ablation/irradiation in liquid: a review. *Advanced Functional Materials, 22*(7), 1333-1353.

Zhang, W. (2014). Nanoparticle aggregation: Principles and modeling. *Nanomaterial: Impacts on Cell Biology and Medicine*, 19-43.